Pole Pitch Optimization of Permanent Magnet Electrodynamic Suspensions in High-Speed Transportation Systems

1st Louis Beauloye
Institute of Mechanics, Materials and Civil Engineering
Université catholique de Louvain (UCLouvain)
Louvain-la-Neuve, Belgium
louis.beauloye@uclouvain.be

2nd Bruno Dehez
Institute of Mechanics, Materials and Civil Engineering
Université catholique de Louvain (UCLouvain)
Louvain-la-Neuve, Belgium
bruno.dehez@uclouvain.be

***Abstract*—Permanent magnet electrodynamic suspensions are good candidates to enable ground transportation systems to reach very high speeds. In these suspensions, the pole pitch of the permanent magnet field source has a significant influence on their performance. This article, therefore, studies qualitatively the impact of performance criteria, whether partial, such as the lift-to-drag ratio, or global, such as the global cost, on the optimal pole pitch. It is shown that the latter depends both on the considered criteria and the operating conditions. In addition, it is pointed out that 3-D models considering the edge effects are essential to derive the optimal pole pitch.**

***Index Terms*—EDS, electrodynamic, suspension, permanent magnet, pole pitch.**

I. Introduction

ELECTRODYNAMIC suspensions (EDSs) are considered to achieve the magnetic levitation of ground transportation systems such as the Hyperloop, a high-speed ground transportation system where small pods travel in evacuated tubes [1]–[3]. This way they can reach very high speeds without any contact and avoid friction losses, as well as vibrations [4].

EDSs are made of a magnetic field source moving with respect to a conductive track. This movement induces eddy currents in the track which react with the magnetic field that produced them to create a force. This force has two components: one in the levitation direction, the lift force, and one in the opposite direction of the movement, the drag force.

Several topologies of EDSs have been considered so far with different tracks [5], [6] and magnetic field sources [7]. Permanent magnet EDSs (PM-EDSs) with a continuous track and a PM Halbach array (HA) have already been deeply studied and optimized. It has been shown that the pole pitch τ has a significant impact on the performance of PM-EDSs [6] and it was therefore used as one of the main parameters to optimize PM-EDSs. To do so, different criteria have been studied such as the lift-to-weight ratio (LWR) [8], the lift-to-drag ratio (LDR) [6] or the ratio between the lift and the total cost of the suspension, including the track [9]. Besides these criteria, different operating conditions and methods were considered. Kublin *et al.* [10] scaled the PM weight to enable the suspension to levitate a given load at a given air gap. However, the load applied on the suspension is generally not taken into account in the optimization while it greatly influences the required dimensions of the suspension. In addition, most studies were done in 2-D without considering the edge effects which can decrease the forces in the system by more than 50% [8]. Finally, the dimensions of the suspension are usually optimized assuming a constant cruising speed. An exception can be found in [2] where Sadeghi *et al.* considered a full trajectory of a pod equipped with PM-EDSs and computed the additional forces during the acceleration and deceleration phases.

In this context, the objective of this work is first to analyze the influence of partial criteria such as the LWR and LDR on the optimum pole pitch of PM-EDSs. It is then to combine these partial criteria into global ones, able to encompass more aspects of PM-EDSs. In Section II, both 2-D and 3-D analytical models used to compute the forces generated in PM-EDSs are presented and validated with numerical simulations. Then, the partial criteria are described in Section III. Finally, in Section IV, global criteria such as the energy consumption and the cost are computed with the help of a case study considering a full trajectory.

II. Modeling

To compute the electromagnetic forces generated in the suspension system illustrated in Fig. 1, a model was first developed in 2-D in the x-y plane. The dimensions are considered infinite in both x and z directions. The model is a Fourier-based model starting from local formulations of Maxwell equations, similar to the one derived in [11]. As a first approach, the PM HA is supposed to be ideal with a sinusoidal magnetization. In this study, the height of the magnet t_m is set to half the pole pitch to have square magnets in a real 2-segment HA. This way, the qualitative analyses in this paper will not be significantly affected when building the real HA.

As stated in [11], the finite dimensions of the HA cause edge effects impacting significantly the forces, by a factor

L. Beauloye is a Research Fellow of the Fonds de la Recherche Scientifique - FNRS

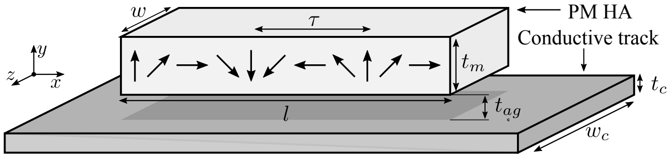

Fig. 1. Permanent magnet electrodynamic suspension with an ideal Halbach array: illustration and parameterization.

TABLE I
PARAMETERS FOR THE MODELS

Parameter	Symbol	Value	Unit
Pole pitch	τ	0.1	m
PM width	w	0.05	m
PM length	l	0.4	m
PM thickness	t_m	0.05	m
Number of pole pairs	p	2	-
Air gap thickness	t_{ag}	0.05	m
Conductive plate thickness	t_c	0.05	m
Remanence	B_r	1.4	T
Track conductivity	σ_c	3.5e7	S/m
Magnet density	ρ	7.5	g/cm^3
Translational speed	v	100	m/s

that can exceed 50%. Only 3-D models can consider these effects. Magneto-dynamic problems in 3-D using finite element methods pose convergence issues, preventing high-speed simulations. They are also computationally expensive as fine meshes are required because of the convergence problem. For this reason, an analytical 3-D model was also implemented. It was developed and described by Chen *et al.* [12]. The lift and drag forces computed with both models are compared to FEM references established using COMSOL Multiphysics® in Fig. 2. The 3-D FEM simulations were only done at low speed because of the convergence problems mentioned above. The parameters used for the validation are listed in Table I. The width of the conductive plate w_c is set to four times the width of the PM array to avoid degradation in the forces. Analytical and numerical predictions match well but there is a significant difference between 2-D and 3-D models. The width of the HA is equal to only half the pole pitch which increases the impact of the transverse edge effects.

The impact of the edge effects on the lift force is depicted in Fig. 3 and 4. They depend on the dimensions of the PM but also the ratio γ between the pole pitch and the air gap. When the PM are closer to the guideway, the impact is less pronounced. These results are in good agreement with the previous studies found in the literature. With a ratio $w/\tau \approx 0.5$ and γ around 5, Cho *et al.* [13], Cho *et al.* [11] and Hu *et al.* [8] found an error around 50% in the forces between 2-D analytical and experimental results. This value is visible in Fig. 3. Only the lift force is depicted because Flankl *et al.* [6] showed that the difference between the LDR evaluated with a simple 2-D model and 3-D FEM is low, meaning that the edge effects have more or less the same impact on the lift and

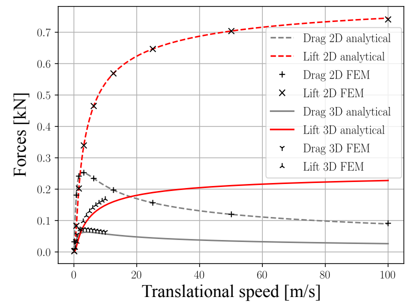

Fig. 2. Lift and drag forces evolution with the translational speed, computed with the 2-D analytical, 2-D FEM, 3-D analytical and 3-D FEM models.

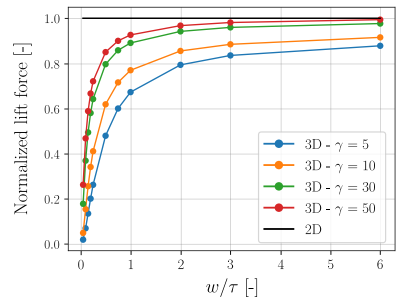

Fig. 3. Lift force per unit of x-y area computed with the 3-D analytical model and normalized with the 2-D approximation for different ratios γ between the pole pitch and the air gap as a function of the ratio between the width of the array and the pole pitch, and for $l/\tau = 4$.

the drag forces.

III. Partial Criteria

As stated in Section I, the optimization of the pole pitch of PM-EDSs can be based on different criteria. Among them, the most common in the literature are the LWR and LDR. The former relates to the PM volume whereas the latter is linked to the efficiency. The power consumption and track volume are also considered. This section investigates the impact of the pole pitch and the track thickness on these criteria, divided into three categories linked to the PM, the operation, and the track.

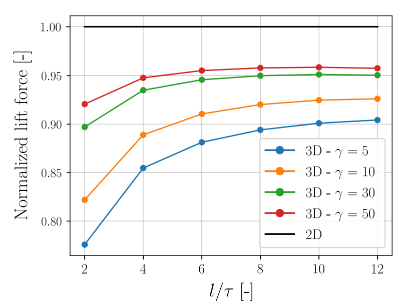

Fig. 4. Lift force per unit of x-y area computed with the 3-D analytical model and normalized with the 2-D approximation for different ratios γ between the pole pitch and the air gap as a function of the ratio between the length of the array and the pole pitch, and for $w/\tau = 3$.

In most papers, the optimization of these criteria is performed on the suspension alone without considering the load or a specific application. In real applications, the lift force must be equal to the sum of the weight W_p of the pod and the weight W_{PM} of the HA. Considering the length is fixed, the width of the PM has then to be adapted according to the pole pitch so as to reach a force compensating the total weight. Because the LWR is independent of w in 2-D, the required width can be computed as:

$$w = \frac{W_p}{\rho g l t_m \left(\mathrm{LWR} - 1\right)} \tag{1}$$

where ρ is the density of the permanent magnets. However, in 3-D, the width must be computed so that it solves a non-linear equation:

$$f(w) = \mathrm{Lift}_{\mathrm{3D}}(w) - \left(W_p + W_{\mathrm{PM}}(w)\right) = 0 \tag{2}$$

with $\mathrm{Lift}_{\mathrm{3D}}$ the lift force computed with the 3D model.

A. PM volume

Optimizing the PM volume for a given load is equivalent to optimizing the LWR which should be equal to the ratio between the total weight and the PM weight. In 2-D, the LWR does not depend on w implying that optimizing the LWR does not require adapting the width. In Fig. 5(a), because of the edge effects, the amount of PM is larger for the same lift and the LWR is reduced when computed in 3-D. The value of the optimum pole pitch is also different depending on the model.

B. Efficiency

When interested in the efficiency of the suspension, the LDR is usually taken as an indicator. As illustrated in Fig. 5(b), the 3-D modeling gives a slightly lower LDR than 2-D modeling because the drag and lift forces are not affected in the exact same way by the edge effects. However, as the total weight changes with the pole pitch, the drag force does not simply vary with $1/\sqrt{\tau}$, which was predicted in [6] but for 2-D modeling.

A more comprehensive criterion, illustrated in Fig. 5(c), is the power consumption, computed from the drag force:

$$P_c = F_{\mathrm{drag}} v = \frac{W_{\mathrm{tot}}}{\mathrm{LDR}} v \tag{3}$$

In 2-D, the weight increase due to the pole pitch is compensated by the decrease in width to have the same lift force, so that the total power consumption decreases. In 3-D, the width does not reduce as much to keep a sufficient level of force and the total power consumption starts to increase above a certain pole pitch. This phenomenon prevents the suspension to have a very large pole pitch as there is no gain in both the power consumption and the total weight of the pod.

The track thickness has also an influence on the efficiency. The variation of the LDR with the track thickness is represented for different pole pitches in Fig. 6. Above a given thickness, the LDR is independent of the track thickness because

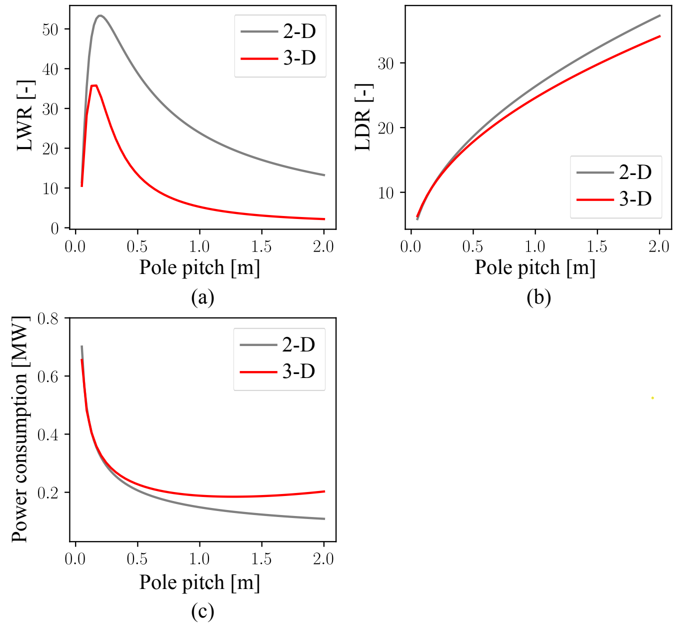

Fig. 5. Criteria as a function of the pole pitch. The simulations are done in 2-D (grey) and in 3-D (red). (a) LWR. (b) LDR. (c) Power consumption.

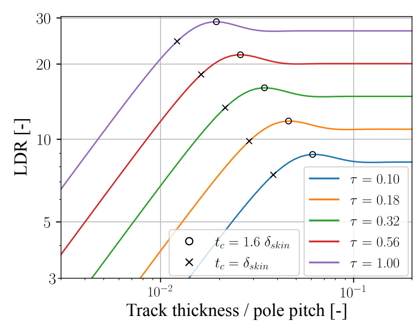

Fig. 6. Variation of the LDR with the track thickness for different pole pitches. The point where the track thickness is equal to the skin depth and to 1.6 times the skin depth are identified with 'x' and 'o' respectively. The latter lead to an increase in the LDR compared to larger track thickness.

of the skin effect. The magnetic field does not penetrate the full conductor but only a depth proportional to the skin depth:

$$\delta_{\mathrm{skin}} = \sqrt{\frac{2\tau}{\pi \mu \sigma_c v}} \tag{4}$$

It is therefore useless to have thick tracks as there is no gain in the power consumption. There is even an optimal thickness increasing the LDR and approximately equal to $t_{c,\,\mathrm{opt}} = 1.6\delta_{\mathrm{skin}}$. This optimum varies with the pole pitch and was also observed by Reitz and Davis [14]. Fig. 7(a) shows that the power consumption is lower with $t_{c,\,\mathrm{opt}}$ for all τ. Thick tracks of constant thickness $t_c = 5$ cm or tracks of varying thickness $t_c = 3\delta_{\mathrm{skin}}$ lead to the same power since they are both much larger than δ_{skin}.

C. Track volume

Thinner tracks mean a smaller cross-section and smaller track cost as represented in Fig. 7(b). The width of the track is proportional to the width of the PM, itself depending on

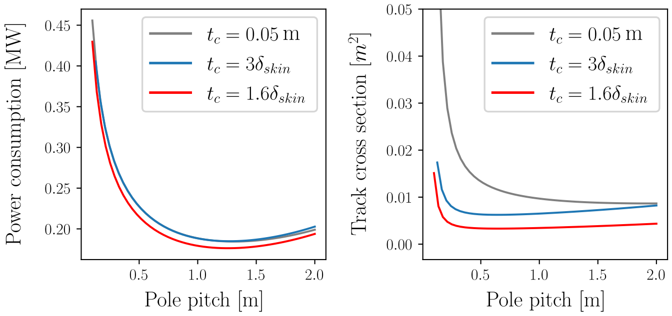

(a) (b)

Fig. 7. Influence of the track thickness on the power consumption (a) and the track cross-section (b), computed considering a varying width of the PM in 3-D.

the pole pitch and the LDR. The track volume including both t_c and w leads thus to an optimum pole pitch. Its value is different if the track thickness is constant or varies with the pole pitch.

IV. Global criteria

As highlighted in the previous section, the LWR, the power consumption, and the track cross-section lead to different optimum pole pitches. A way to combine all three is to consider global criteria such as the total cost or the total energy consumption. In this section, global criteria are computed from these partial ones based on a case study considering a complete trajectory rather than travel at a constant speed.

A. Definition

The energy consumption of one pod per travel E_p is computed from the integral, approximated as a sum, of the drag, acceleration, and deceleration forces over the trajectory. To compute this energy as a function of the pole pitch, a special scheme, represented in Fig. 8, must be adopted. From the parameters, the width of the HA is computed with the Newton-Raphson method and (2), to be able to sustain the total weight of the pod at the cruising speed v. The energy is then computed with these dimensions on each segment of a speed profile, presented in the next section, which is discretized to achieve a numerical evaluation. The lift force varies on each segment due to the speed evolution and so does the effective air gap, that is computed from the following equation:

$$g(t_{ag,i}) = \text{Lift}_{\text{3D}}(t_{ag,i}) - \text{W}_{tot} = 0 \quad (5)$$

through the Newton-Raphson method. If all the air gaps are above a minimum air gap, fixed to 10 mm, then the total energy is computed. If not, this means that this pole pitch leads to an unfeasible solution with the selected high-speed air gap at the cruising speed.

Two global criteria, the total cost and the total energy consumption, are defined to combine the three partial criteria. The former is the sum of the costs of the PMs, the conductive track, and the operation cost during a variable period of time:

$$C_{\text{tot}} = M_{\text{PM}} C_{\text{PM}} + \frac{\text{E}_p \; N_t \; 365 \; N_y}{3.6\text{e}6} C_{\text{E}} + \frac{M_c C_c}{N_p} \quad (6)$$

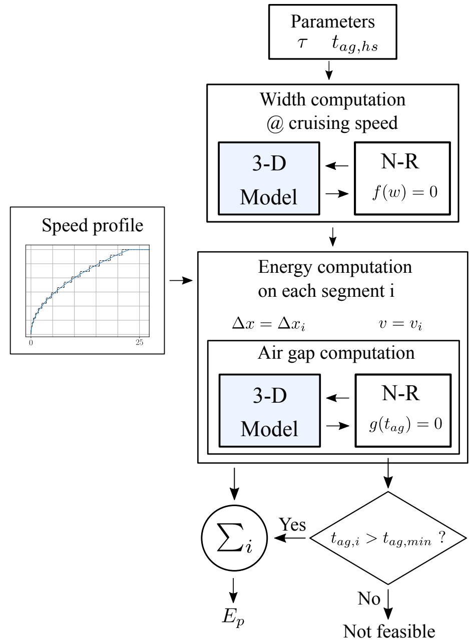

Fig. 8. Computation scheme of the energy consumption per pod per travel from the parameters and the discretized speed profile.

where M_{PM} is the mass of the PMs, C_{PM} is the cost of the PMs, N_t is the number of travels per pod per day, N_y is the number of year of operation, C_{E} is the cost of the energy, M_c is the mass of the track, C_c is the cost of the track and N_p is the number of pods. The latter considers the energy required to produce the rare-earth magnets and the aluminum of the track as well as the operating energy:

$$E_{\text{tot}} = M_{\text{PM}} E_{\text{PM}} + \text{E}_p \; N_t \; 365 \; N_y + \frac{M_c E_c}{N_p} \quad (7)$$

B. Case study parameters

The parameters used in the present case study are summarized in Table II. The material parameters of the suspension are listed in Table I. The pods follow a speed profile where the acceleration and deceleration are equal. This profile, depicted in Fig. 10, is discretized in smaller segments where the speed can be considered constant. The lift force in PM-EDSs is sufficient to sustain the weight of the pod only above a given speed, the lift-off speed. Below that speed, the pods rely on wheels which fix the air gap at a relatively high value [2], set to 30 cm in this case study. The wheels oppose a rolling resistance to the movement. It is neglected since it is much lower than the magnetic resistance, even considering the worst-case with rubber tires [15], [16]. The mass of the pod M_p without its suspensions is 15t. There are four suspensions per pod. Only the conductive part of the track is taken into account in further computations. The track is considered to have two parts, one under each side of the pod, that are three times wider than the PM array, as illustrated in Fig. 9. The number of travels per pod per day is equal to:

$$N_t = \frac{N_h \; 60}{T_p \; N_p} \; 2 = 16 \quad (8)$$

TABLE II
GLOBAL PARAMETERS OF THE CASE STUDY

Parameter	Symbol	Value	Unit
Travel time	T	1	h
Cruising speed	v	300	m/s
Acceleration	a	2	m/s^2
Lift-off speed	v_{lf}	10	m/s
High-speed air gap	$t_{ag,hs}$	0.03	m
Time between pods	T_p	3	min
Number of pods	N_p	40	-
Number of hours per day	N_h	16	-
Number of years	N_y		-
Cost PM	C_{PM}	250	\$/kg
Cost energy	C_{E}	0.112	\$/kWh
Cost track	C_c	3.5	\$/kg
Energy production PM	E_{PM}	375	MJ/kg
Energy production track	E_c	150	MJ/kg
Mass pod	M_p	15	t
Number of suspensions	N_s	4	-

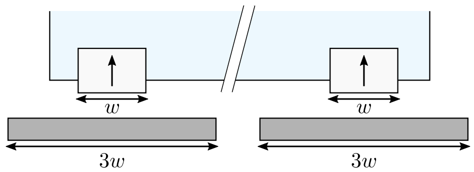

Fig. 9. Schematic view of the bottom of the pod (light blue) with the two sides of the track (dark gray). Each side is three times wider than the corresponding PM array.

where N_h is the number of hours of operation per day and T_p is the time in minutes between two consecutive pods. The result is multiplied by two to consider the round trip. The costs of the PMs and the track are only the material costs of the rare-earth magnets and the aluminum. The energy cost is a value found for early 2022. The PM and track energies are approximated from the life cycle analysis of the production of NdFeB rare-earth permanent magnets [17] and the production of aluminum [18].

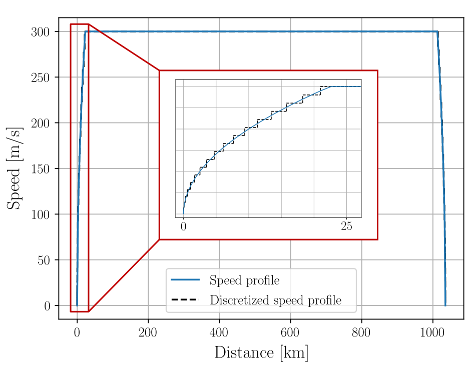

Fig. 10. Speed profile of the travel as a function of the distance. The acceleration and deceleration are assumed to be constant. The profile is discretized (dashed line) and the speed is considered constant on each segment.

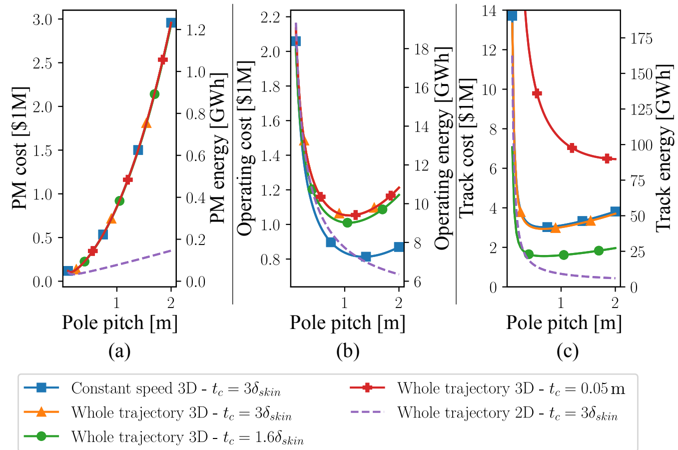

Fig. 11. Cost and energy as a function of the pole pitch computed with a 2-D (purple) or a 3-D model, considering a constant speed (blue) or a whole trajectory and with different track thicknesses (orange-green-red). (a) for the PM. (b) for the operation. (c) for the track.

C. Results

The three parts of the cost and the energy are depicted in Fig. 11, computed with the parameters of Table II and for 1 year of operation. The results are presented for different speed profiles, track thickness and models. First, it can be seen that the edge effects have a significant impact on the results as none of the three costs is well approximated in 2-D. The minimum in the operating cost indeed appears only with a 3-D model. As stated before, the optimum pole pitch depends on the criteria used. The cost of the magnets, linked to the LWR, is minimum for small pole pitches, as shown in Fig. 11(a). The speed profile on the whole trajectory has a significant impact on operating cost, as illustrated in Fig. 11(b). The cost is indeed higher and the minimum moves towards lower values of the pole pitch since the acceleration and deceleration forces are proportional to the mass of the magnets. However, the pole pitch minimizing the operating cost is rather independent of the track thickness. The track cost, represented in Fig. 11(c), can be significantly reduced when choosing a track thickness depending on the speed and the pole pitch. Besides, a track thickness equal to $1.6\delta_{\mathrm{skin}}$, in green, leads to a slightly lower operating cost and lower track cost. The energy consumption in Fig. 11 follows an identical evolution with the pole pitch as the cost but the relative difference between the three parts are different.

The pole pitch minimizing the total cost and energy consumption depends on the number of years of operation because the part linked to the operation will become predominant. Fig. 12 depicts the optimum pole pitch as a function of the number of years of operation. The stair shape is due to the discretization of the pole pitch vector. For each pole pitch, several dozens of evaluations of the 3-D model are indeed needed. Since there is no minimum in the operating energy computed with the 2-D model, the optimum pole pitch is the maximum one. In 3-D, it converges towards the minimum of the operating energy when the number of years increases. In contrast, for a short operating time, the pole pitch is lower

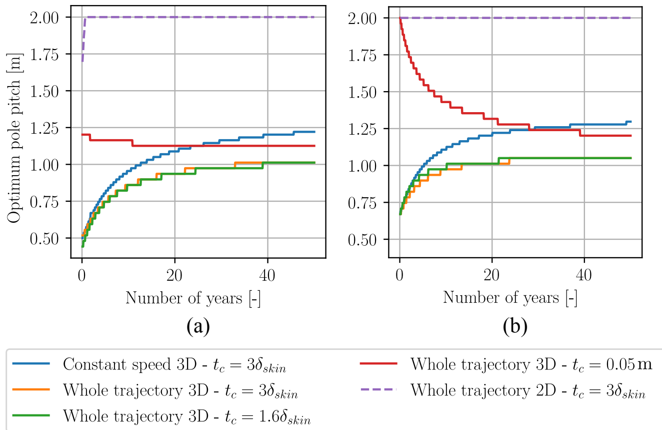

Fig. 12. Pole pitch minimizing the total cost (a) and energy consumption (b) as a function of the number of years of operation. It is computed with a 2-D (purple) or a 3-D model, considering a constant speed (blue) or a whole trajectory, and with different track thicknesses (orange-green-red).

given that the suspension cost is no longer negligible. As stated before, the acceleration and deceleration phases also make the pole pitch converge towards lower values. The track thickness has a significant impact on the optimal pole pitch. With a fixed track thickness equal to 5 cm, the cost or the energy of the track dominates for a small number of years of operation. When the thickness of the track varies with the pole pitch and the speed, the proportionality coefficient between the skin depth and the track thickness does not influence significantly the optimal pole pitch, unlike the resulting cost and energy consumption.

V. Conclusion

This work investigated the impact of the models, the criteria, the operating conditions and the track thickness on the pole pitch optimization of PM-EDSs. 2-D models do not capture the edge effects which have a strong influence on the results. 3-D models need therefore to be used to compute quantities such as the forces and the power consumption. Besides, the lift-to-weight and the lift-to-drag ratios often used in the literature can be part of an optimization criterion but are not sufficient to take all the aspects of the suspension together into account. To overcome this limitation, the total cost and energy consumption encompassing a part linked to the magnets, the operation, and the track are proposed. By applying these to a case study, it is shown that adding the acceleration/deceleration phases tends to shorten the pole pitch. An optimum track thickness can be found for a specific pole pitch to enhance both the energy consumption and the track cost compared to a thick track. The optimum pole pitch depends on the balance between magnets, track, and operation and thus on the operating conditions such as the time of utilization. Finally, let us point out that the parameters of the case study influence the value of the optimal pole pitch because the relative importance of the different parts of the global criteria could change but this will not impact the qualitative analyses and general conclusions drawn in this paper.

References

[1] E. Chaidez, S. P. Bhattacharyya, and A. N. Karpetis, "Levitation Methods for Use in the Hyperloop High-Speed Transportation System," *Energies*, vol. 12, no. 21, p. 4190, Jan. 2019.

[2] S. Sadeghi, M. Saeedifard, and C. Bobko, "Dynamic Modeling and Simulation of Propulsion and Levitation Systems for Hyperloop," in *2021 13th International Symposium on Linear Drives for Industry Applications (LDIA)*, Jul. 2021, pp. 1–5.

[3] J. K. Nøland, "Prospects and Challenges of the Hyperloop Transportation System: A Systematic Technology Review," *IEEE Access*, vol. 9, pp. 28 439–28 458, 2021.

[4] H.-W. Lee, K.-C. Kim, and J. Lee, "Review of maglev train technologies," *IEEE Transactions on Magnetics*, vol. 42, no. 7, pp. 1917–1925, Jul. 2006.

[5] R. Post and D. Ryutov, "The Inductrack: a simpler approach to magnetic levitation," *IEEE Transactions on Applied Superconductivity*, vol. 10, no. 1, pp. 901–904, Mar. 2000.

[6] M. Flankl, T. Wellerdieck, A. Tüysüz, and J. W. Kolar, "Scaling laws for electrodynamic suspension in high-speed transportation," *IET Electric Power Applications*, vol. 12, no. 3, pp. 357–364, 2018.

[7] T. N. França, H. Shi, Z. Deng, and R. M. Stephan, "Overview of Electrodynamic Levitation Technique Applied to Maglev Vehicles," *IEEE Transactions on Applied Superconductivity*, vol. 31, no. 8, pp. 1–5, Nov. 2021.

[8] Y. Hu, Z. Long, J. Zeng, and Z. Wang, "Analytical Optimization of Electrodynamic Suspension for Ultrahigh-Speed Ground Transportation," *IEEE Transactions on Magnetics*, vol. 57, no. 8, pp. 1–11, Aug. 2021.

[9] S. Hasanzadeh, H. Rezaei, and E. Qiyassi, "Analysis and Optimization of Permanent Magnet Dimensions in Electrodynamic Suspension Systems," *J Electr Eng Technol*, vol. 13, pp. 307–314, 2018.

[10] T. Kublin, L. Grzesiak, P. Radziszewski, M. Nikoniuk, and L. Ordyszewski, "Reducing the Power Consumption of the Electrodynamic Suspension Levitation System by Changing the Span of the Horizontal Magnet in the Halbach Array," *Energies*, vol. 14, no. 20, p. 6549, Jan. 2021.

[11] H.-W. Cho, H.-S. Han, J.-S. Bang, H.-K. Sung, and B.-H. Kim, "Characteristic analysis of electrodynamic suspension device with permanent magnet Halbach array," *Journal of Applied Physics*, vol. 105, no. 7, p. 07A314, Apr. 2009.

[12] Y. Chen, W. Zhang, J. Z. Bird, S. Paul, and K. Zhang, "A 3-D Analytic-Based Model of a Null-Flux Halbach Array Electrodynamic Suspension Device," *IEEE Transactions on Magnetics*, vol. 51, no. 11, pp. 1–5, Nov. 2015.

[13] H. Cho, D. K. Bae, H.-K. Sung, and J. Lee, "Experimental Study on the Electrodynamic Suspension System With HTSC and PM Halbach Array Magnets," *IEEE Transactions on Applied Superconductivity*, vol. 18, no. 2, pp. 808–811, Jun. 2008.

[14] J. R. Reitz and L. C. Davis, "Force on a Rectangular Coil Moving above a Conducting Slab," *Journal of Applied Physics*, vol. 43, no. 4, pp. 1547–1553, Apr. 1972.

[15] A. A. Popov, D. J. Cole, C. B. Winkler, and D. Cebon, "Laboratory measurement of rolling resistance in truck tyres under dynamic vertical load," *Proceedings of the Institution of Mechanical Engineers, Part D: Journal of Automobile Engineering*, vol. 217, no. 12, pp. 1071–1079, Dec. 2003.

[16] M. Guo, X. Li, M. Ran, X. Zhou, and Y. Yan, "Analysis of Contact Stresses and Rolling Resistance of Truck-Bus Tyres under Different Working Conditions," *Sustainability*, vol. 12, no. 24, p. 10603, Dec. 2020.

[17] B. Sprecher, Y. Xiao, A. Walton, J. Speight, R. Harris, R. Kleijn, G. Visser, and G. J. Kramer, "Life Cycle Inventory of the Production of Rare Earths and the Subsequent Production of NdFeB Rare Earth Permanent Magnets," *Environ. Sci. Technol.*, p. 8, 2014.

[18] P. Nunez and S. Jones, "Cradle to gate: life cycle impact of primary aluminium production," *The International Journal of Life Cycle Assessment*, vol. 21, no. 11, pp. 1594–1604, Nov. 2016.